# Hydrothermal events in the Linzizong Group: Implications for Paleogene exhumation and paleoaltimetry of the southern Tibetan Plateau

Wentao Huang [a,b,c,d,*], Peter C. Lippert [c], Peter W. Reiners [b], Jay Quade [b], Paul Kapp [b], Morgan Ganerød [e], Zhaojie Guo [f], Douwe J.J. van Hinsbergen [g]

[a] Key Laboratory of Continental Collision and Plateau Uplift, Institute of Tibetan Plateau Research, and Center for Excellence in Tibetan Plateau Earth Sciences, Chinese Academy of Sciences, Beijing 100101, China
[b] Department of Geosciences, University of Arizona, Tucson, AZ, 85721, USA
[c] Department of Geology and Geophysics, University of Utah, Salt Lake City, UT, 84112, USA
[d] Department of Earth and Environmental Sciences, University of Rochester, Rochester, NY, 14627, USA
[e] Centre for Geodynamics, Geological Survey of Norway, Leiv Eirikssons vei 39, 7491 Trondheim, Norway
[f] Key Laboratory of Orogenic Belts and Crustal Evolution, Ministry of Education, School of Earth and Space Sciences, Peking University, Beijing, China
[g] Department of Earth Sciences, Utrecht University, Princetonlaan 8a, 3584 CB Utrecht, the Netherlands

## ARTICLE INFO

## ABSTRACT

Knowledge of the thermal history of the Linzizong Group (69–47 Ma) within the Gangdese arc is critical for interpreting the geologic evolution and isotope-based paleoaltimetric results of the southern Lhasa terrane of the Tibetan Plateau. Here, we combine results from geochronologic and thermochronologic studies of this group (divided into Dianzhong, Nianbo, and Pana formations upsection) and the structurally overlying Qianggeren granite ($\sim$52 Ma) in the Linzhou basin. Whole rock $^{40}$Ar/$^{39}$Ar ages of volcanic rocks from the stratigraphically lower Dianzhong and Nianbo formations are $\sim$10 Myr younger than their corresponding zircon U-Pb ages, suggesting a thermal disturbance of the argon system. Zircon (U-Th)/He ages (ZHe, 63 dates) range from 54 to 24 Ma, and apatite (U-Th-Sm)/He ages (AHe, 43 dates) range from 27 to 4 Ma. Inverse modeling of the thermochronologic data from the Qianggeren granite indicates rapid cooling between 42 and 26 Ma, possibly induced by movement of the Gulu-Hamu thrust. Positive correlations between ZHe ages and effective uranium and other geologic observations provide evidence that the Dianzhong and Nianbo formations were heated 300 °C at 54–50 Ma, and that the entire Linzizong Group was variably heated to 130–170 °C at 42–27 Ma. These findings, together with published geochronologic and thermochronologic data, suggest that abundant 50–45 Ma zircon fission track and ZHe ages from the Gangdese arc likely reflect conductive cooling of the Gangdese arc after a $\sim$52 Ma magmatic flare-up episode rather than rapid regional exhumation. Areas far from Cenozoic faults and deeply incised river valleys in southern Tibet have experienced only $\sim$3 km of exhumation since 45 Ma, consistent with the establishment of a low-relief, plateau-like physiography by Eocene time. The (hydro)thermal events are also manifested by widespread calcite recrystallization and $\delta^{18}$O and $\Delta_{47}$ alteration in most carbonates from the Linzizong Group, which must be taken into account in past and future carbonate-based paleoaltimetric studies.

© 2022 Elsevier B.V. All rights reserved.

## 1. Introduction

The growth of the Tibetan Plateau played a critical role in the geodynamics and paleoclimate of Asia (e.g., Molnar et al., 1993), and global climate via chemical weathering and carbon storage (e.g., Raymo and Ruddiman, 1992). As such, establishing the surface uplift history of the Tibetan Plateau has been a major and challenging focus of study. Geologic studies indicate that the crust of the Lhasa and Qiangtang terranes (Fig. 1a) was shortened by $\sim$50% during Cretaceous time, which implies substantial crustal thickening and likely surface uplift prior to the onset of the India-Asia collision (e.g., Kapp et al., 2007). Quantitative and semi-quantitative determination of the elevation history of the Tibetan Plateau principally relies on reconstructions of the stable
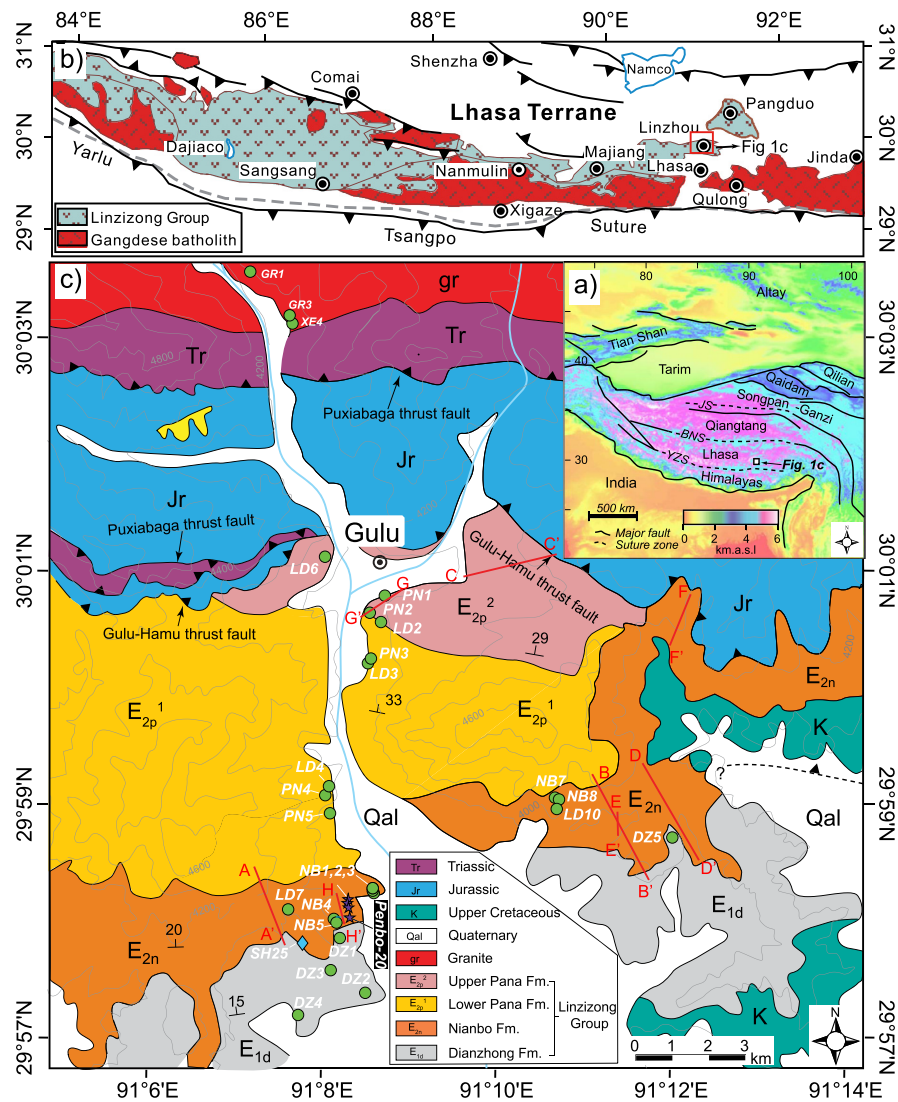
**Fig. 1.** (a) Location of the study area indicated on a digital elevation model of the India-Asia collision zone, modified from Dupont-Nivet et al. (2010). (b) Simplified geological map showing the distribution of the Gangdese batholith and associated Linzizong Group in the southern Lhasa terrane, modified from Lee et al. (2009). (c) Geologic map of the Linzhou basin with sampling localities indicated. Purple stars: zircon U-Pb dating; green circles: zircon, apatite (U-Th)/He dating; blue diamond: whole rock $^{40}Ar/^{39}Ar$ dating. Red lines represent sections studied for stable and clumped isotope: sections AA', BB', and CC' are from Ding et al. (2014), sections DD', EE', FF', and GG' are from Ingalls et al. (2018), and section HH' is from Quade et al. (2020). YZS, Yarlung Zangbo suture; BNS, Bangong-Nujiang suture; JS, Jinsha suture. (For interpretation of the colors in the figure(s), the reader is referred to the web version of this article.)

isotopic compositions of ancient meteoric water, surface temperature, and fossil records. Results from these methods widely support the presence of a >4 km surface elevation of the Gangdese mountains in the southern Lhasa terrane by the early Miocene (<20 Ma) (e.g., Khan et al., 2014; Currie et al., 2016). For the critical Paleogene time window, however, during which continental collision initiated (e.g., Hu et al., 2015), and the Indian monsoon system developed (Licht et al., 2014), paleoaltitude estimates range from near-sea level to >4 km (e.g., Rowley and Currie, 2006; Wei et al., 2016; Ingalls et al., 2018). This uncertainty in our understanding of the surface elevation of the Tibetan Plateau led Ding et al. (2014) and Su et al. (2019) to speculate that a deep, E-W trending paleo-valley system (<2.3 km elevation) existed during Paleogene time between the >4 km high Gangdese mountains to the south and the >4 km Tanggula mountains to the north.

The deformation and exhumation history of the Qiangtang and northern Lhasa terranes are consistent with the formation of a relatively high elevation and low relief proto-plateau by Eocene time and the northward and southward growth of the plateau thereafter. For example, apatite (U-Th-Sm)/He (AHe) and fission track

(AFT) ages from the Qiangtang and northern Lhasa terranes and the thermal modeling of these ages indicate most samples were exhumed to depths of <3 km by 45 Ma, after which they were exhumed to the surface at a rate of <0.05 mm/yr. AHe and AFT ages are younger (Oligocene – Miocene) in the southern Lhasa terrane and interpreted to record mid-Cenozoic exhumation related to uplift in the hanging wall of the Gangdese thrust and subsequent river incision (Rohrmann et al., 2012; Laskowski et al., 2018, and references therein). When plateau-like conditions were established in the southern Lhasa terrane remains an open question. Zircon (U-Th)/He (ZHe) and fission track (ZFT) results from the Gangdese batholith and unreset Gangdese region-derived detritus reveal two main age groups (Laskowski et al., 2018, and references therein; Shen et al., 2019). An Oligocene-early Miocene age group probably represents cooling related to Gangdese thrust activity and river incision, similar to the AHe and AFT ages described above. An older late Paleocene-early Eocene age group is interpreted to reflect either conductive cooling after magmatic emplacement (Wang et al., 2015; Shen et al., 2019) or exhumation related to Tibetan shortening (Ge et al., 2016; Li et al., 2016). The former interpretation

implies that erosional exhumation of the Gangdese arc has been limited since the Eocene, whereas the latter interpretation requires that >6 km of rock has been removed from the southern Lhasa terrane at an erosional exhumation rate of 0.14-0.7 mm/yr.

Stable isotopic evidence supporting that the Gangdese mountains were >4 km high by 52 Ma has primarily come from rocks within the Linzizong Group in the Linzhou basin (sections AA'-GG', Fig. 1c, Ding et al., 2014; Ingalls et al., 2018). Recent evaluation of the oxygen, carbon, and clumped isotopic records from carbonates exposed across the southern plateau region found that many isotopic records for paleoaltimetry, including the carbonates from the Linzizong Group in the Linzhou basin (section HH' in Fig. 1c), may have been reset due to later burial and heating (Quade et al., 2020). Low $\delta^{18}O$ values in calcite may indicate precipitation at high elevation, but secondary calcite formed or altered at elevated temperatures of 50-100 °C can show similar values. Discriminating between temperature and elevation effects in carbonate chemistry is challenging, yet it is essential to reconstruct reliable paleoelevations. Thus, independent characterization of the thermal history of the carbonates can clarify the interpretation of isotope records used to reconstruct temperature and paleoelevation.

Although the Linzizong Group is widespread across much of the southern Lhasa terrane, it has not been targeted for systematic low-temperature thermochronologic studies (Fig. 1b). Here, we apply zircon U-Pb, bulk rock $^{40}Ar/^{39}Ar$, ZHe, and AHe geochronology and thermochronology to reconstruct the thermal history of the Linzizong Group in the Linzhou basin. We also compile published geochronologic and thermochronologic results of the Gangdese arc and combine thermochronologic results with stable and clumped isotopic results to assess the growth and rise of the southern Lhasa terrane during early Paleogene time.

## 2. Geological background and sampling

The Lhasa terrane is separated from the Indian plate-derived Himalayan fold-thrust belt by the Yarlung-Tsangpo suture to the south, and from the Qiangtang terrane by the Late Jurassic–Early Cretaceous Banggong-Nujiang suture to the north (Fig. 1a). The southern margin of the Lhasa terrane exposes the east-west trending Gangdese arc, dominated by the Mesozoic to Eocene Gangdese batholith and *ca.* 69-40 Ma Linzizong volcanic-sedimentary sequence (Fig. 1b). The Linzizong Group is well exposed in the Linzhou basin, where it has a total thickness of 3500 m and lies unconformably above the folded and thrusted Upper Cretaceous Takena Formation red beds (He et al., 2007) (Fig. 1c). In the Linzhou area, the Linzizong Group is divided, from bottom to top, into the Dianzhong, Nianbo, and Pana formations (BGMRXAR, 1993), which are separated by two slightly angular unconformities (Figs. 1 and 2). The Dianzhong Formation ($E_{1d}$) is comprised of 270 m of andesitic lavas, dacitic to rhyolitic ash-tuff layers and ignimbrite/pyroclastic flows. The 330 m-thick Nianbo Formation ($E_{2n}$) mainly consists of mudstone, conglomerate, and limestone in the lower part, and calcareous sandstone intercalated with rhyolitic tuff in the upper part. The Pana Formation is predominantly brown-gray dacitic ignimbrites in its lower part ($E_{2p}^{1}$, 1900 m thick), with volcaniclastic sandstone interbedded with rhyolitic tuff in its upper part ($E_{2p}^{2}$, 1050 m thick). Basaltic dikes pervasively intrude $E_{1d}$ and $E_{2n}$, and the underlying Cretaceous strata. The Linzizong Group is in the footwall of the north-dipping Gulu-Hamu thrust fault; this thrust carries Triassic and Jurassic marine carbonates in its hanging wall (Fig. 1c). The 52 Ma Qianggeren granite (Fig. 2a) of the Gangdese batholith intrudes the Triassic strata. The Qianggeren granite, the ignimbrite and tuff from the $E_{2p}^{2}$, and upper $E_{2p}^{1}$, and the dikes intruding $E_{1d}$ and $E_{2n}$ show little evidence of hydrothermal alteration (Figs. 2a-d). In contrast, ignimbrites from the lower $E_{2p}^{1}$, tuff from the $E_{2n}$, and lavas from

$E_{1d}$ exhibit pervasive hydrothermal alteration; this hydrothermal alteration is strongest in haloes along the margins of the dikes and along the unconformities (Figs. 2e-h, j-l).

Previous geochronologic studies of the Linzizong Group, associated dikes, and the Qianggeren granite include results from zircon U-Pb (LA-ICP-MS and SIMS methods) and $^{40}Ar/^{39}Ar$ (whole rock, alkali feldspar, plagioclase, hornblende, biotite) techniques (Zhou et al., 2004; Yue and Ding, 2006; He et al., 2007; Lee et al., 2007; Chen et al., 2014; Ding et al., 2014; Huang et al., 2015a; Zhu et al., 2015; Chen et al., 2016) (Fig. 4, Table S3). These data indicate eruption or deposition of $E_{1d}$ at 69-58 Ma, $E_{2n}$ at 58-52 Ma, and $E_{2p}$ at 52-47 Ma. Crosscutting dikes in the Takena Formation, $E_{1d}$ and $E_{2n}$, and the Qianggeren granite were mainly intruded at ∼52 Ma. Previous thermochronologic studies of the Linzhou area only focused on the Qianggeren granite. Biotite and K-feldspar $^{40}Ar/^{39}Ar$ studies suggest slow cooling of the Qianggeren granite at temperatures >300 °C between 49 and 42 Ma, followed by an episode of more rapid cooling to temperatures <150 °C beginning at ∼42 Ma (He et al., 2007). Apatite (U-Th-Sm)/He dates of the granite are 16-12 Ma and have been interpreted to reflect the timing of deep river incision in the area (Rohrmann et al., 2012; Ingalls et al., 2018). The thermal history of the Linzizong Group has not been previously investigated in detail. A reset whole rock $^{40}Ar/^{39}Ar$ age of a lava sample from $E_{1d}$ suggests that these rocks were heated to ∼300 °C (Huang et al., 2015a) and vitrinite reflectance of a shale sample from $E_{2n}$ suggests that these strata reached temperatures >135 °C (Ingalls et al., 2018).

For this study, we collected four samples (Penbo-20, Shar1-20, Shar1-99, and Shar1-177) from tuff layers in the lower $E_{2n}$ for zircon U-Pb geochronology, and one sample (SH25) from a rhyolitic tuff layer at the bottom of $E_{2n}$ for $^{40}Ar/^{39}Ar$ whole rock geochronology (Fig. 1c). We also collected 25 samples for zircon and apatite (U-Th)/He thermochronology: four lava samples (DZ1-DZ4) from $E_{1d}$; four sandstone samples (NB2, NB4, NB7, LD7) and three tuff samples (NB3, NB8, LD10) from $E_{2n}$; nine ignimbrite and tuff samples (LD2-LD4, LD6, PN1-PN4) from $E_{2p}$; two samples (DZ5, NB5) are from dikes, and three samples (GR1, GR3, XE4-4) from the Qianggeren granite (Fig. 1c). Methods for geochronology and thermochronology, as well as stratigraphic level of each of these samples, can be found in the supplementary material.

## 3. Results

Zircons from the four samples of the $E_{2n}$ tuff layers are euhedral without inherited cores. Zircon U-Pb ages are displayed in Figs. 3a-d and Table S1. For sample Penbo-20, the 15 concordant ages (52–61 Ma) from individual grains provide a weighted mean age of 55.8 ± 0.8 Ma ($1\sigma$, mean square weighted deviation (MSWD) = 1.6). For sample Shar1-20, 24 concordant ages (47.5–61.6 Ma) give a weighted mean age of 54 ± 1.4 ($1\sigma$, MSWD = 1.5). For sample Shar1-99, the 27 concordant ages (51.6–71.6 Ma) provide a weighted mean age of 58.7 ± 1.5 Ma ($1\sigma$, MSWD = 1.6). For sample Shar1-177, the 42 concordant ages (50.7–72.4 Ma) provide a weighted mean age of 55.4 ± 0.8 Ma ($1\sigma$, MSWD = 0.97). These ages are indistinguishable except that of Shar1-99, indicating that the $E_{2n}$ was deposited quickly.

The $^{40}Ar/^{39}Ar$ whole rock apparent age spectrum and inverse isochron age results of sample SH25 are presented in Fig. 3e and Table S2. Similar to the age spectrum of sample SH01 described in Huang et al. (2015a), the age spectrum of SH25 also shows a high degree of disturbance with a MSWD of 42.67; therefore the weighted mean plateau age of 47.8 ± 1.0 Ma must be interpreted with caution. Zircon U-Pb dating constrains the deposition of the entire Linzizong Group to 69-47 Ma. $^{40}Ar/^{39}Ar$ and U-Pb ages from similar stratigraphic levels are generally indistinguishable, except
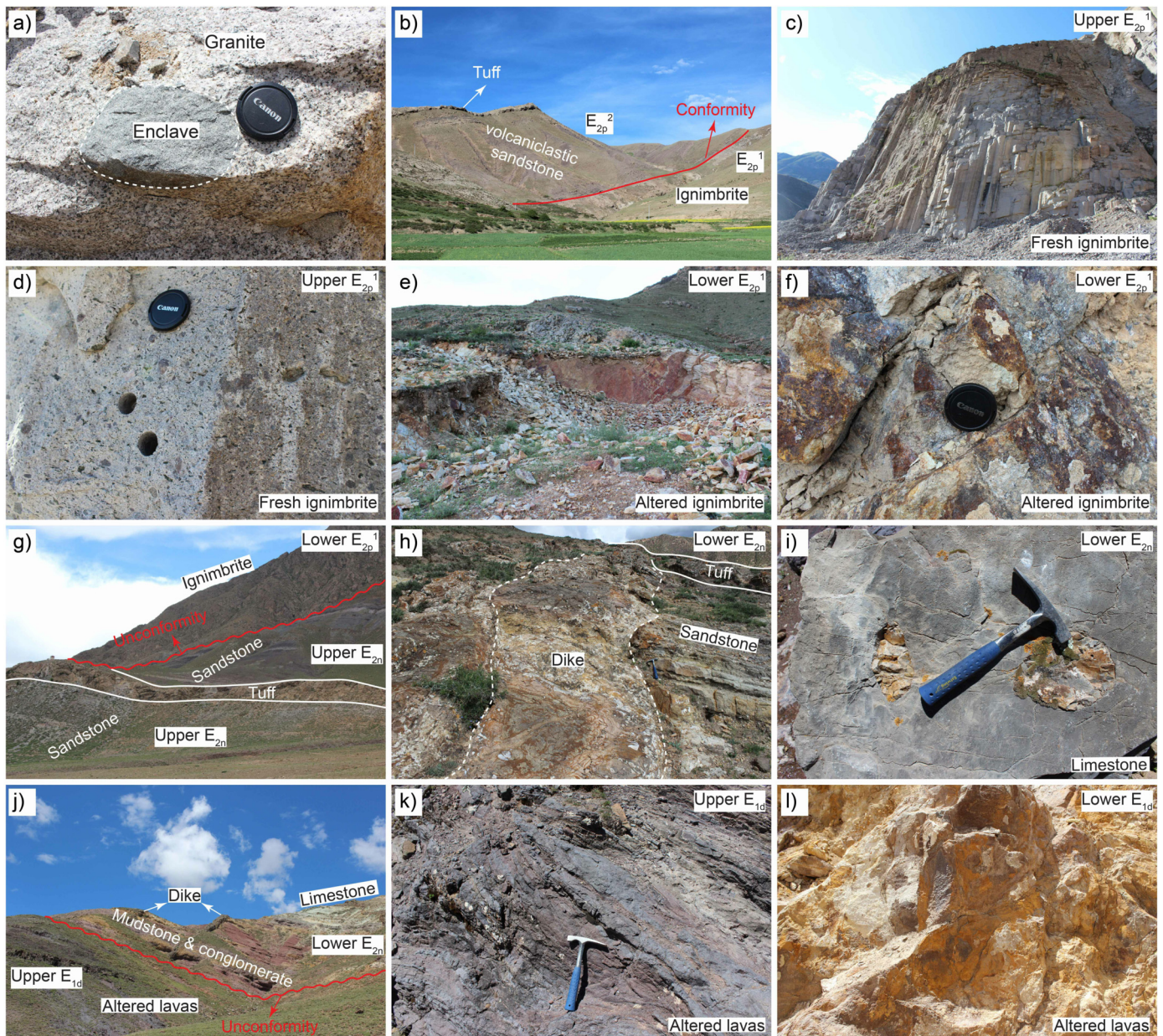
**Fig. 2.** Field observations of the Linzizong Group and Qianggeren granite in the Linzhou basin. The $E_{1d}$, $E_{2n}$, and the lower $E_{2p}^1$ show outcrop evidence for extensive hydrothermal chemical alteration, whereas the upper $E_{2p}^1$ and $E_{2p}^2$ do not. $E_{1d}$, Dianzhong Formation; $E_{2n}$, Nianbo Formation; $E_{2p}^1$, lower Pana Formation; $E_{2p}^2$, upper Pana Formation.

for two samples (SH25 in this study and SH01 in Huang et al. (2015a)) in which their whole rock $^{40}Ar/^{39}Ar$ ages are 48–51 Ma, that is, ~10 Myr younger than zircon U-Pb ages of the same rocks. These $^{40}Ar/^{39}Ar$ ages are similar to the ~52 Ma crystallization ages of the dikes, the granite, and the ignimbrites in the $E_{2p}^1$ unit (Fig. 4).

We acquired 43 new AHe ages from 15 samples collected from the Linzizong Group, dikes, and the Qianggeren granite (Fig. 4, Table S5), supplementing the 10 published AHe ages from the granite (Rohrmann et al., 2012; Ingalls et al., 2018). The majority of AHe dates from the Linzizong Group and the granite are 16-4 Ma with younger ages deeper in the section. We note that four AHe ages from the $E_{2p}^1$ ignimbrite are ~20 Ma (Fig. 4, Tables S5).

We also acquired 63 ZHe ages from 25 samples from the Linzizong Group, dikes, and the granite; some of these samples also yielded the AHe ages described above (Fig. 4, Table S4). ZHe dates of the granite are 37-33 Ma; these are significantly younger than

the ~52 Ma zircon U-Pb age of the granite. ZHe dates from the $E_{2p}^2$ and upper $E_{2p}^1$ units are 45-52 Ma and statistically indistinguishable from zircon U-Pb and $^{40}Ar/^{39}Ar$ dates from the same samples. This distribution of ZHe ages from the $E_{2p}^2$ and upper $E_{2p}^1$ unit indicates that the temperature of these volcanic rocks never exceeded 170 °C after emplacement (Reiners et al., 2004). That is, these ZHe ages are not reset. In contrast, ZHe dates from the $E_{1d}$, $E_{2n}$, and lower $E_{2p}^1$ units vary widely from 24 to 54 Ma. These ZHe dates also show positive correlations with the concentration of effective uranium (eU, U + 0.235 x Th). This correlation is consistent with He loss from low-damage grains, in which He diffusion decreases and closure temperature increases with increasing radiation damage as fast helium diffusion pathways are blocked by radiation damage zones (Guenthner et al., 2013). Such a He loss is possibly due to slow-cooling or reheating sometime more recently than their ZHe maximum age of ~52 Ma (Figs. 6, 7).
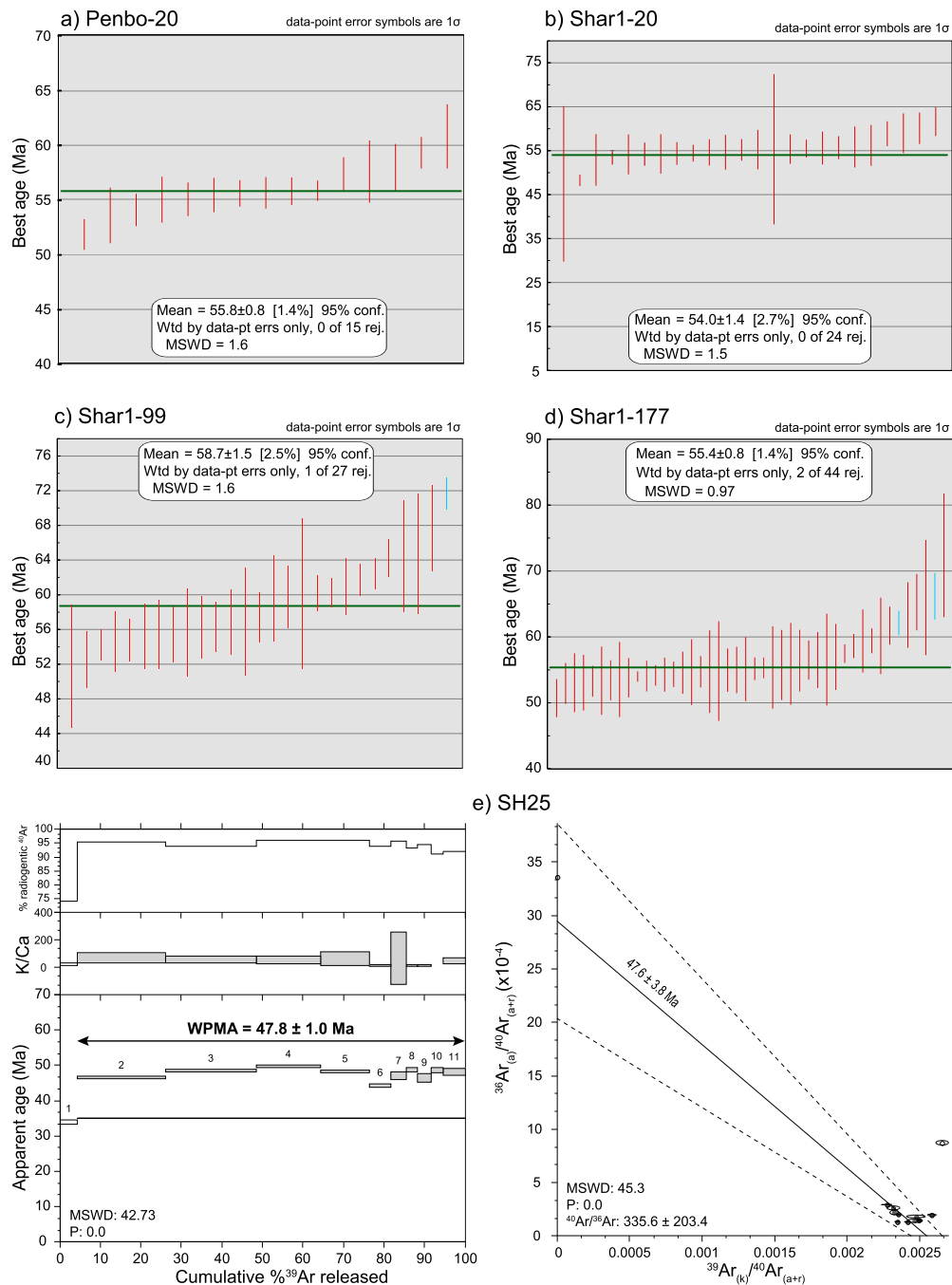
**Fig. 3.** Zircon U-Pb and whole rock $^{40}Ar/^{39}Ar$ geochronology of the volcanic samples from the lower $E_{2n}$. Stratigraphic levels for Shar1-177, 1-99, 1-20, Penbo-20, and SH25 are 285 m, 290 m, 369 m, 447 m, and 284 m, respectively (Table S3). (a-d) Individual zircon U-Pb ages and their weighted mean ages. (e) Whole rock $^{40}Ar/^{39}Ar$ age spectra, percent radiogenic argon, and K/Ca ratio determined as a function of the cumulative %$^{39}Ar$ released (left), and inverse isochrons (right). In the inverse isochron diagram, steps with open symbols were not used in the isochron age calculation. MSWD: mean square of weighted deviates.

## 4. Thermal history modeling and identification of thermal events

### 4.1. Modeling strategy

We applied both inverse and forward modeling of the apatite and zircon He ages using the HeFTy thermochronologic modeling program (Ketcham, 2005; Guenthner et al., 2013) to constrain the possible thermal history of the Linzhou basin. For our inverse models of the thermal history of the Qianggeren granite, we define the constraint boxes using: (1) intrusion of the granite at 51.9±2.5 Ma at 700–800 °C as indicated by zircon U-Pb ages (He et al., 2007); (2) biotite $^{40}Ar/^{39}Ar$ ages of 49 ± 0.17 Ma at 250-350 °C (He et

al., 2007); (3) K-feldspar $^{40}Ar/^{39}Ar$ ages of 45-35 Ma at 150-350 °C (He et al., 2007); (4) zircon He ages of 37-32.5 Ma at 140-220 °C; (5) apatite (U-Th-Sm)/He ages of 16-10 Ma at 40-60 °C; and (6) a surface temperature of 10 °C at 0 Ma.

We also applied forward modeling to constrain the thermal history of the Qianggeren granite and the Linzizong Group. We favor the forward modeling approach for the Linzizong Group because inverse modeling uses averaged grain-specific inputs (i.e., grain size, U and Th concentrations), assumes well-constrained sources of the data variation, and only displays modeled date-eU correlations for the best-fit time-temperature (t-T) paths. We modeled the positive correlations between zircon He ages and eU concentration
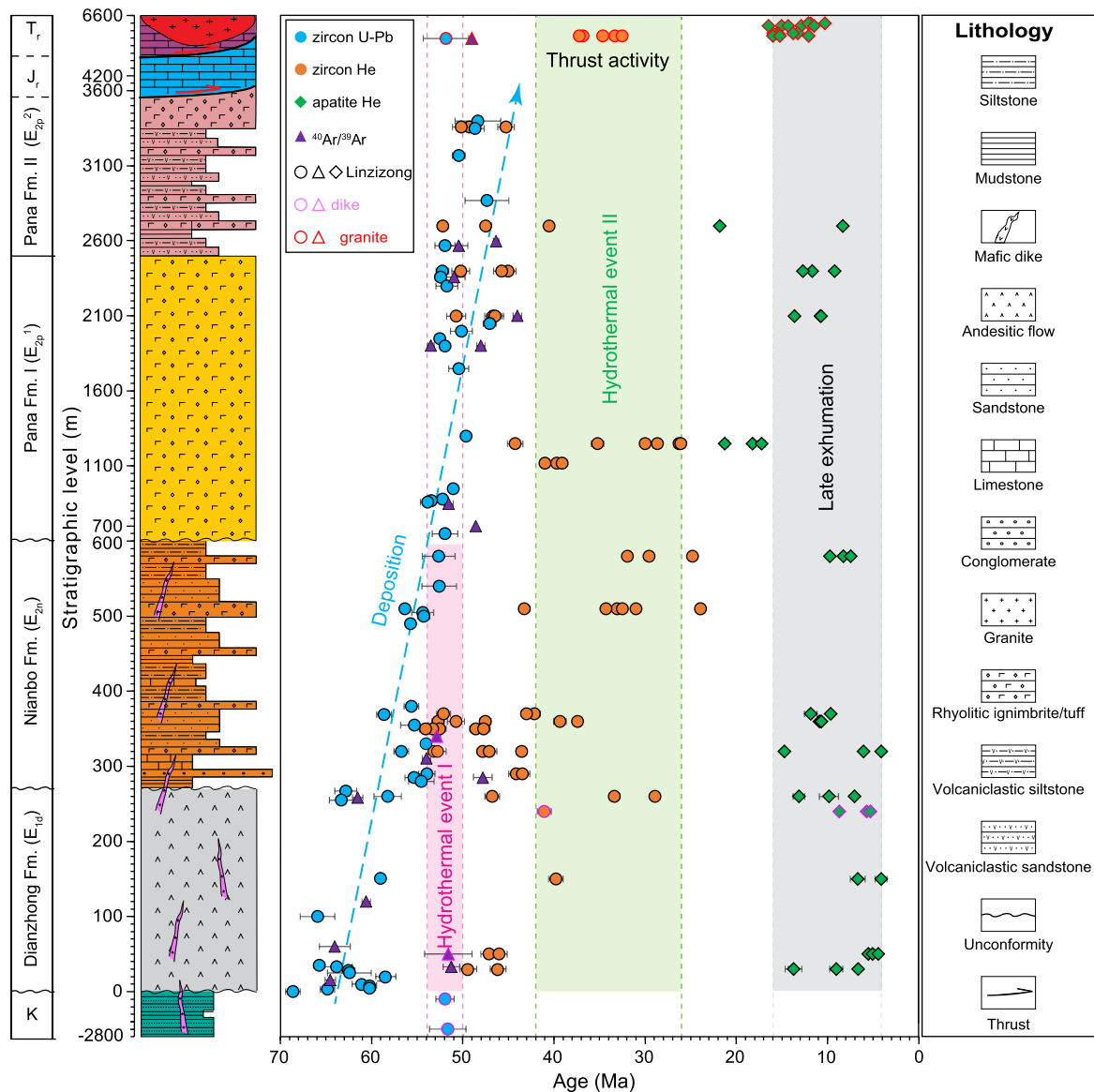
**Fig. 4.** Geochronologic and thermochronologic results of the Linzizong Group, associated dikes, and structurally overlying Qianggeren granite in the Linzhou area. Zircon U-Pb ages, $^{40}$Ar/$^{39}$Ar ages, zircon (U-Th)/He dates, and apatite (U-Th-Sm)/He dates are plotted along the stratigraphic section. Four zircon U-Pb ages and one whole rock $^{40}$Ar/$^{39}$Ar ages are from the lower $E_{2n}$ presented in Fig. 3; other zircon U-Pb ages (n = 47) and $^{40}$Ar/$^{39}$Ar ages (n = 16) are from previous studies (see Table S3 for references). All ZHe ages (Tables S4) and most AHe ages (Tables S5) are from this study. The ten AHe ages of the Qianggeren granite are reported by Rohrmann et al. (2012) and Ingalls et al. (2018). Shaded areas represent the timing of thermal events described in Section 5; height of shaded area represents the Linzhou basin stratigraphy affected by each thermal event. K: Upper Cretaceous Takena Formation; $J_r$: Jurassic marine strata, $T_r$: Triassic marine strata.

using the radiation damage accumulation and annealing model implemented in HeFTy (Guenthner et al., 2013). The retentivity of He in zircon initially increases with radiation damage accumulation before a critical threshold, leading to positive correlation between single grain He ages and their eU concentration.

The input parameters for forward modeling include grain size, U and Th concentrations, and t-T paths. We binned samples from the granite into a single group (Fig. 5b), whereas samples from the Linzizong Group were binned into six groups (Figs. 6, 7) according to stratigraphic level: $E_{2p}^2$ and upper $E_{2p}^1$ units (mean stratigraphic level of 2500 m, PN1, LD2, LD3, LD6), lower $E_{2p}^1$ unit (mean stratigraphic level of 1200 m, PN5, LD4), upper $E_{2n}$ (mean stratigraphic level of 550 m, NB8, LD10), lower $E_{2n}$ (mean stratigraphic level of 350 m, NB2, NB3, NB4, LD7), upper $E_{1d}$ (stratigraphic level of 260 m, DZ1), and lower $E_{1d}$ (mean stratigraphic level of 50 m, DZ2, DZ4).

The thermal history constraint for the forward modeling of the Qianggeren granite is from its inverse modeling results. We applied the following constraints on the forward modeling of the Linzizong Group. First, the whole rock $^{40}$Ar/$^{39}$Ar ages (SH1 and SH25, Table S3) from the bottom of $E_{1d}$ and $E_{2n}$ are reset, but single-crystal plagioclase $^{40}$Ar/$^{39}$Ar ages (D-3, XL156, LZ9913, N-9, Table S3) from the $E_{1d}$ and $E_{2n}$ are consistent with eruption/depositional ages of the sequence constrained by zircon U-Pb dating. This indicates that these strata may have been heated to a temperature above the closure temperatures for the argon system in andesitic whole rock, but below the closure temperatures of the plagioclase grains. These picked and dated plagioclase grains (0.25-0.45 mm) by Zhou et al. (2004) and Chen et al. (2014) are the larger bound of feldspar in the whole rock, and thus have higher closure temperatures than the whole rock. We estimate that this temperature is ~300 °C based on experimental studies showing the closure temperatures of feldspar of 200-400 °C, depending on gain size and
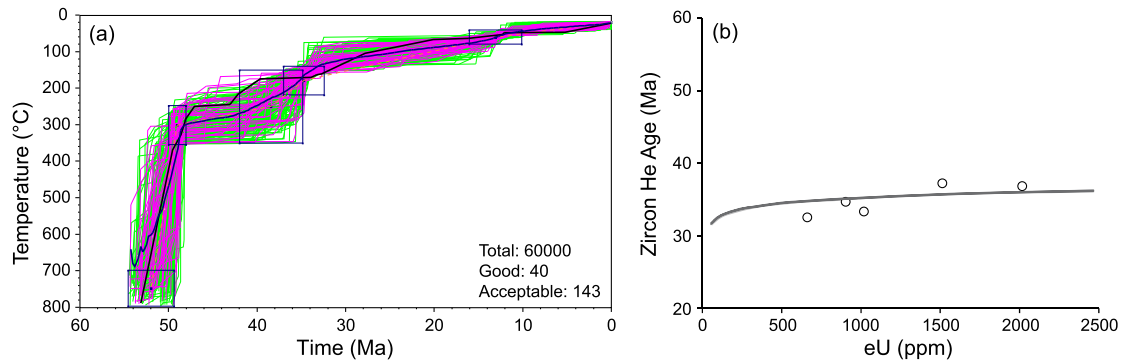
**Fig. 5.** Results from thermal history models of the Qianggeren granite. (a) Results from inverse modeling using HeFTy. Pink paths: good fit; green paths: acceptable fit; blue line: weighted mean of good and acceptable fit paths; black line: best fit path; blue boxes: time-temperature constraints described in Section 4. (b) Output of forward modeling based on the determined thermal history inferred from inverse modeling in (a) indicates that the modeled curves ($60 \pm 10$ μm) are a good fit to the measured dataset. The output contains a central curve (for mean zircon grain size of 60 μm with a shaded envelope ($\pm 2$ grain size standard deviations, 10 μm). The resulting envelopes almost overlap with the central curve because the grain size variation of the dated zircon grains is small.

cooling rate (Cassata and Renne, 2013). This thermal event that led to diffusional loss of argon in the whole rock, was likely related to eruption of the ignimbrite in the $E_{2p}^1$ unit, and intrusion of crosscutting dikes and the Qianggeren granite at ~52 Ma. We used a typical geothermal gradient of 25 °C/km as our second constraint. For the third constraint, we assumed no overburden for strata younger than $E_{2p}$. Our fourth constraint is the assumption of a surface temperature of 10 °C. Model returns using these parameters suggest that the thermal history for $E_{1d}$ and $E_{2n}$ before ~48 Ma is characterized by conductive heating that peaked at ~52 Ma. This modeling suggests $E_{1d}$ and $E_{2n}$ then experienced fast cooling within one million years, followed by burial heating induced by the newly deposited $E_{2p}$ strata. We designed a series of t-T inputs with different scenarios after 48 Ma to estimate (1) when the subsequent heating (as indicated by the reset ZHe ages) and cooling initiated, (2) the longevity of these heating and cooling episodes, and (3) the peak temperature reached for each unit of the Linzizong Group.

### 4.2. Modeling results

Results from our inverse modeling of the Qianggeren granite in Fig. 5a suggest slow cooling of the granite before 42 Ma, followed by an episode of rapid cooling through a temperature window of approximately 300-100 °C at 42–26 Ma. We attribute this fast cooling to erosional exhumation induced by rock uplift during movement of the Gulu-Hamu thrust (He et al., 2007). After 26 Ma, the granite cooled slowly (~0.1 mm/yr) to the surface temperature, which we attribute to regional river incision. This thermal history results in a good fit between the modeled ZHe age-eU-grain size distribution and measured ZHe-eU pairs in the forward modeling (Fig. 5b).

Forward modeling of the positive ZHe ages-eU patterns of each unit of the Linzizong Group was applied jointly with AHe results (Figs. 6, 7). Movement along the Gulu-Hamu thrust beginning at ~42 Ma may have caused further (structural) burial of the footwall Linzizong Group. Hence, we designed the t-T paths with additional heating that initiates at ~42 Ma. Slow cooling of the Linzizong Group related to regional exhumation initiated at 26 Ma, as revealed by the inverse modeling of the Qianggeren granite. We were unable to find a single t-T path that fit the thermochronometric data from our six groups of stratigraphically separated samples when the only variation between the t-T paths was a linear increase in temperature between the sample sets proportional to the stratigraphic distance between them. This suggests that heating effects other than that due to change in geothermal gradient is required to explain the thermochronometric ages observed in our

samples. This is further evidenced by the presence of the youngest ZHe ages from samples in the upper $E_{1d}$, upper $E_{2n}$, and lower $E_{2p}^1$, which suggests that these units could have been heated to higher temperatures than those of other units. A source of heat in addition to burial is thus required.

We first examined the thermochronologic data from the lower Pana I unit. Eight ZHe dates from this unit show a good positive ZHe-eU correlations (Fig. 6). The four youngest ZHe ages range from 29 to 26 Ma (Table S4), suggesting that peak heating close to 170 °C (ZHe closure temperature) could have occurred during this time period. We then used an iterative process in which we continually changed the time (29, 28, 27 Ma) when peak temperature of 170 °C could have been reached (Fig. 6a). We also modeled a peak temperature of 160, 180, and 190 °C at 27 Ma (Fig. 6e). The designed t-T path with peak temperature of 170 °C occurred at 27 Ma results in envelopes of modeled ZHe ages-eU-grain size distributions covering the largest number of the observed ZHe-eU pairs (Figs. 6b-d, f-h).

Although the peak temperatures experienced by different units of the Linzizong Group may vary, the timing of peak heating was likely synchronous. Therefore, we applied the same approach described in the paragraph above to determine the maximum temperatures of other Linzizong units at ~27 Ma. Results from our models suggest peak temperatures of 130 °C for the lower $E_{1d}$, 145 °C for the upper $E_{1d}$, 130 °C for the lower $E_{2n}$, 170 °C for the upper $E_{2n}$ and the lower $E_{2p}^1$, and 150 °C for the upper $E_{2p}^1$ and entire $E_{2p}^2$ (Figs. 6, 7). The t-T paths of the preferred models which fit the largest number of the measured data suggest that a second episode of heating of the Linzizong Group occurred from 42 to 27 Ma, with peak temperatures at 27 Ma, and rapid cooling from 27 to 26 Ma (Fig. 8). After 26 Ma, the Linzizong Group cooled slowly until ~10 Ma. Four AHe ages from the $E_{2p}^1$ ignimbrite are ~20 Ma; these apatite crystals may have higher closure temperatures due to their larger grain sizes (Fig. 4, Tables S5). We attribute the ~20 Ma ages to the cooling process after the second episode of heating rather than the later exhumation. Positive AHe and eU correlation is only observed in two samples. However, the predicted AHe age-eU-grain size distribution from our preferred t-T paths covers about half of the measured AHe-eU pairs (Fig. S1).

Base on the results of our forward modeling, we interpret that the Linzizong Group was heated first between 54 and 50 Ma and then again between 42 and 27 Ma (Fig. 8). Heating of the $E_{1d}$ and $E_{2n}$ to 300 °C and the field observations of extensive chemical alteration halos in these rocks (Figs. 2g-l) indicate that the first heating (thermal event I) involved hydrothermal fluid flow. We attribute the source of these hot fluids to the eruption of the ~1.9 km thick overlying $E_{2p}^1$ ignimbrites, and the intrusion of dikes
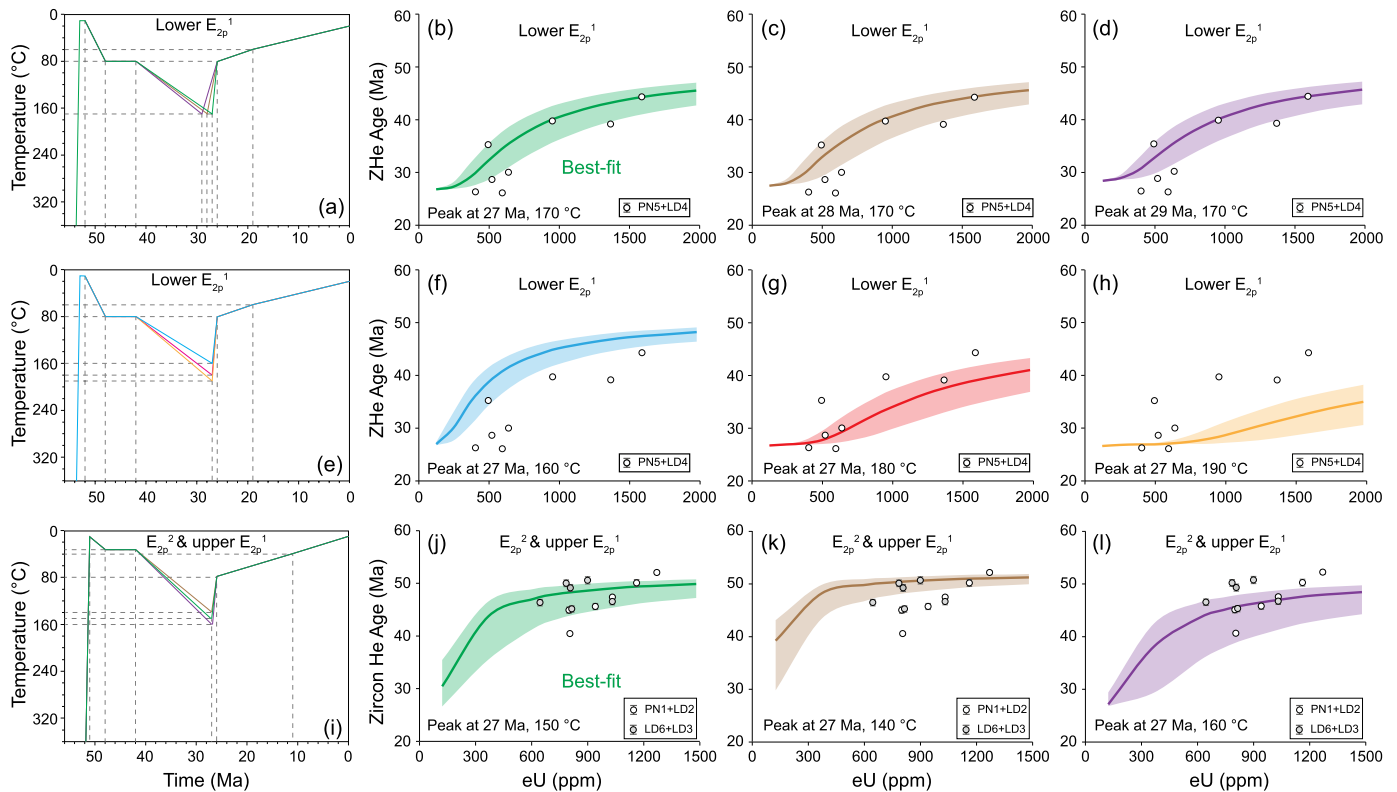
**Fig. 6.** Forward thermal modeling of the $E_{2P}$ from the Linzizong Group based on positive zircon He age-eU trends. (a) Designed t-T paths testing the timing (27, 28, 29 Ma) peak heating to 170 °C was reached for the lower $E_{2P}{}^1$. (b-d) Modeled ZHe-eU envelopes using the thermal histories shown in (a) and measured eU-ZHe pairs for the lower $E_{2P}{}^1$. (e) t-T paths illustrating alternative peak temperatures (160, 180, 190 °C) reached at 27 Ma for the lower $E_{2P}{}^1$. (f-h) Modeled ZHe-eU envelopes using the thermal histories shown in (e) and measured eU-ZHe pairs for the lower $E_{2P}{}^1$. (i) Designed t-T paths testing peak temperatures (140, 150, 160 °C) reached at 27 Ma for the $E_{2P}{}^2$ & upper $E_{2P}{}^1$. (j-l) Modeled ZHe-eU envelopes using the thermal histories shown in (i) and measured eU-ZHe pairs for the $E_{2P}{}^2$ & upper $E_{2P}{}^1$. The modeled envelopes shown in (b) and (j), which combine the effects of grain size and radiation damage, cover the largest number of the measured ZHe-eU pairs. Thus, their corresponding t-T paths are the preferred thermal histories for lower $E_{2P}{}^1$, and $E_{2P}{}^2$ & upper $E_{2P}{}^1$, respectively. Modeled grain sizes are 48±14 μm for the lower $E_{2P}{}^1$, and 48±24 μm for the $E_{2P}{}^2$ & upper $E_{2P}{}^1$. The output contains the central curves (mean grain size) and a shaded envelop (±2 standard deviations of the mean grain size). Color of the modeled ZHe-eU envelopes is consistent with that of the corresponding designed t-T path. White circles represent data with clear positive zircon He age-eU correlation. Grey circles are from samples without clear positive zircon He age-eU correlation; they also mostly fall within the resulting envelopes in the preferred model. Details of the geologic events and corresponding constraints on the best-fit paths can be found in Table S6.

and the Qianggeren granite at ∼52 Ma. The second heating event induced non-uniform depth-temperature reheating with what appears to be a quasi-reversed geothermal gradient. Stratigraphic intervals (lower $E_{2p}{}^1$ and upper $E_{2n}$) along the unconformity between the $E_{2n}$ and $E_{2p}$ were heated to 170 °C (Figs. 6a-h, 7a-d). The upper $E_{1d}$ interval below the unconformity between $E_{1d}$ and $E_{2n}$ was heated to 145 °C, in contrast to the immediately adjacent units which were heated to 130 °C (Figs. 7e-l). We observed substantial hydrothermal alteration in the lower $E_{2p}{}^1$ unit (Figs. 2e-f). The second heating event was also coeval with the rapid cooling of the Qianggeren granite (Fig. 8). We speculate that the younger heating event (thermal event II) was caused by a combination of burial and hot fluid flow along permeable unconformities in the section during prolonged heating and fluid migration associated with active thrusting and structural burial in the footwall of the Gulu-Hamu thrust.

## 5. Discussion

### 5.1. Thermal event I and plateau development in the southern Lhasa terrane during the early Paleogene

Hydrothermal fluid circulation related to magmatism and faulting in geologically active regions can extensively reset thermochronometers (e.g., Ault et al., 2016; Abbey et al., 2018). We suggest that $E_{1d}$ and $E_{2n}$ experienced significant heating as a result of eruption/emplacement of igneous rocks and hydrothermal

fluid flow. Whole rock $^{40}Ar/^{39}Ar$ ages from $E_{1d}$ and $E_{2n}$ are reset to 51 and 48 Ma, respectively. These ages are younger than the deposition ages (69-55 Ma) of the strata but overlap or are slightly younger than the eruption age of the 1900 m thick $E_{2p}{}^1$ ignimbrite sequence, and the ages of the dikes (52-50 Ma) that cut across the $E_{1d}$ and $E_{2n}$ strata (Fig. 4), and the ∼52 Ma age of Qianggeren granite. This is consistent with the whole rock $^{40}Ar/^{39}Ar$ ages being either completely reset by the heating event or representing the initiation age of cooling after the heating event.

The unreset ZHe ages of 47-48 Ma of the four samples (LD3, LD2, PN1, and LD6) from the upper $E_{2p}{}^1$ and $E_{2p}{}^2$ (Table S4) further indicate that the Linzizong Group has not been heated to >170 °C since ∼50 Ma. This limits post-depositional exhumation of the Linzizong Group to less than ∼6 km, which contrasts to the previous estimation of 6-9 km for the southern Lhasa terrane (e.g., Ge et al., 2016; Li et al., 2016). We examine this discrepancy in the magnitude of regional exhumation in greater detail by compiling the published geochronologic and thermochronologic results of the Gangdese batholith and Linzizong Group from the southern Lhasa terrane (Fig. 9). Eruption of the $E_{2p}{}^1$ ignimbrite and intrusion of the dikes and Qianggeren granite in the Linzhou basin were coeval with a magmatic flare-up across the Gangdese arc (spanning 85-95° E longitude) at ∼52 Ma (e.g., Lee et al., 2009; Zhu et al., 2015) (Figs. 9a, b). Cooling ages from fission track (ZFT) analysis of zircon from the Gangdese batholith and from sediment eroded from the Gangdese region are most abundant at ∼50 Ma (Fig. 9c). The
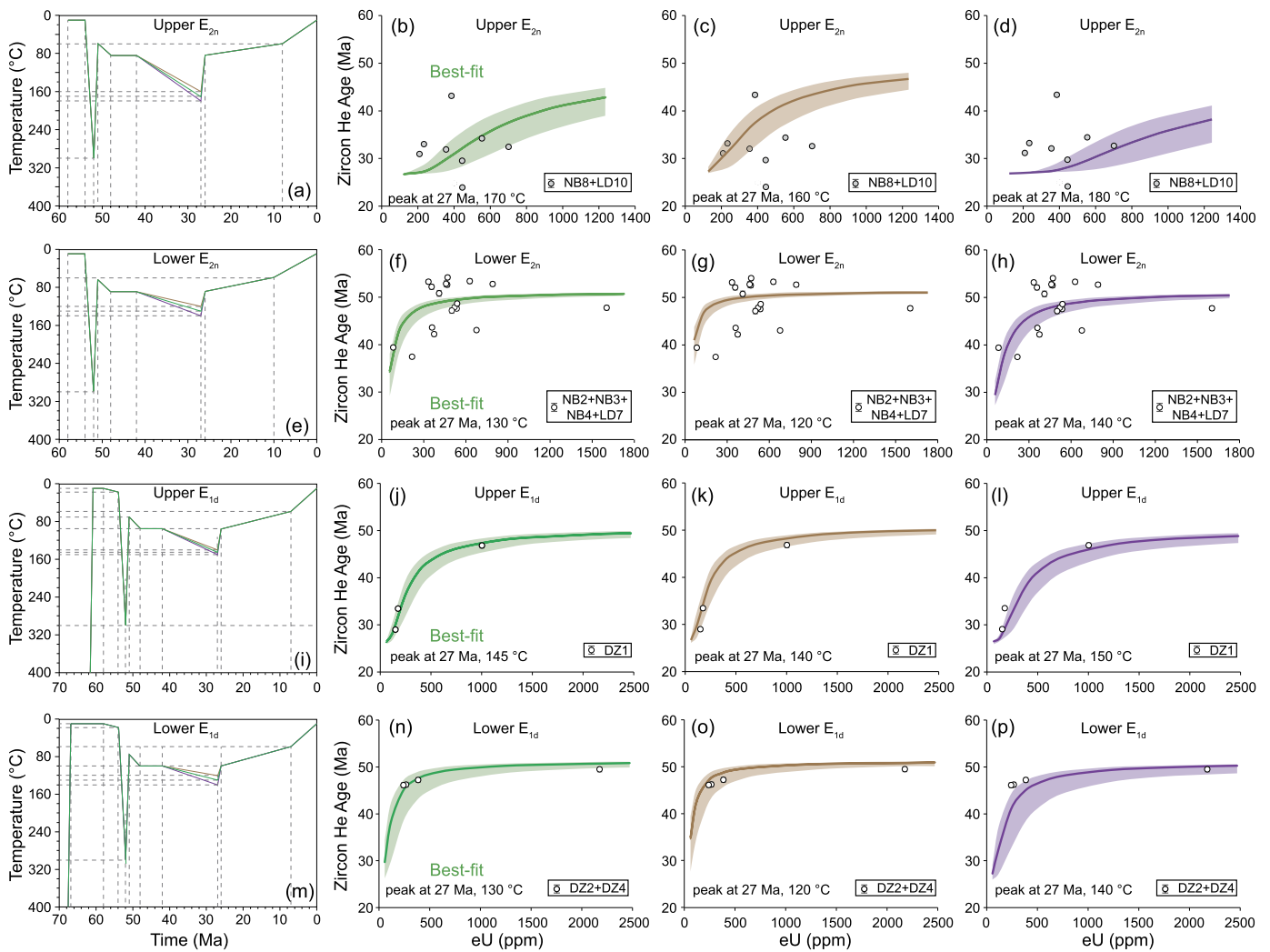
**Fig. 7.** Forward thermal modeling of the $E_{1d}$ and $E_{2n}$ from the Linzizong Group based on positive zircon He age-eU trends. (a) Representative t-T paths testing peak temperatures (160, 170, 180 °C) reached at 27 Ma for the upper $E_{2n}$. (b-d) Modeled ZHe-eU envelopes using the thermal histories shown in (a) and measured eU-ZHe pairs for the upper $E_{2n}$. (e) Designed t-T paths testing peak temperatures (120, 130, 140 °C) reached at 27 Ma for the lower $E_{2n}$. (f-h) Modeled ZHe-eU envelopes using the thermal histories shown in (e) and measured eU-ZHe pairs for the lower $E_{2n}$. (i) Designed t-T paths testing peak temperatures (140, 145, 150 °C) reached at 27 Ma for the upper $E_{1d}$. (j-l) Modeled ZHe-eU envelopes using the thermal histories shown in (i) and measured eU-ZHe pairs for the upper $E_{1d}$. (m) Designed t-T paths testing peak temperatures (120, 130, 140 °C) reached at 27 Ma for the lower $E_{1d}$. (n-p) Modeled ZHe-eU envelopes using the thermal histories shown in (m) and measured eU-ZHe pairs for the lower $E_{1d}$. The modeled envelopes shown in (b), (f), (j), and (n), which combine the effects of grain size and radiation damage, cover the largest number of the measured ZHe-eU pairs. Their corresponding t-T paths are thus the preferred thermal histories. Modeled grain sizes are $50\pm16$ μm, $60\pm22$ μm, $35\pm10$ μm, and $45\pm22$ μm for the upper $E_{2n}$, lower $E_{2n}$, upper $E_{1d}$, and lower $E_{1d}$, respectively. The output contains the central curves (mean grain size) and a shaded envelop ($\pm2$ standard deviations of the mean grain size). Color of the modeled ZHe-eU envelopes is consistent with that of the corresponding designed t-T path. White circles represent data with clear positive zircon He age-eU correlations. Grey circles are samples from the upper $E_{2n}$ without clear positive zircon He age-eU correlations. The thermal history, except the peak temperature, of this unit is inferred from the preferred thermal history solutions of the strata above and below with stratigraphic level considered. "Peak" refers to the highest temperatures reached during the second hydrothermal event. Details of the geologic events and corresponding constraints on the best-fit paths can be found in Table S6.

distributions of ZHe ages of the Gangdese batholith and the reset ZHe ages of the Linzizong Group both peak at ~46 Ma (Figs. 9d, e). Therefore, similar to our interpretation that the whole rock $^{40}Ar/^{39}Ar$ and ZHe ages of the $E_{1d}$ and $E_{2n}$ in the Linzhou basin record hydrothermal resetting associated with magmatic emplacement, it is very likely that these ZFT and ZHe age distributions of the regionally extensive Gangdese batholith are attributed to cooling of the Gangdese arc after the magmatic flare-up. We also note that the peak magmatic flare-up age (~52 Ma) is slightly older than the peak ZFT age (~50 Ma) and the peak ZHe age (~46 Ma) (Figs. 9a-d). This may be due to their different closure temperatures as the flare-up waned and potential thermal events after the flare-up which partially annealed the ZFT and ZHe ages.

Such an early Eocene ZFT and ZHe age group of the Gangdese arc was previously interpreted to represent regional exhumation due to uplift of the Tibetan Plateau at the early stage of the

India-Asia collision (e.g., Ge et al., 2016; Li et al., 2016). Erosional exhumation of 6-9 km since ~50 Ma and exhumation rates >0.15 mm/yr for the Gangdese arc were thus suggested. Here, we argue that these ages reflect cooling of the Gangdese arc after the magmatic flare-up. With reheating due to the magmatic flare-up accounted for, our revised interpretation is that erosional exhumation of the Gangdese arc was of lower magnitude and at lower rates in Eocene. Although conductive heating related to magmatic flare-up at ~52 Ma may have wiped most thermochronologic records of the Gangdese arc before that time, the reported few older ZFT and ZHe ages (77-56 Ma, Figs. 9c, d) indicate that the Gangdese arc underwent rapid cooling and exhumation during the Cretaceous to Paleocene time. Such a transition from rapid exhumation in the Cretaceous to Paleocene time to very slow exhumation in the Eocene time for the southern Lhasa terrane was similar to that of the Qiangtang terrane and northern Lhasa ter-
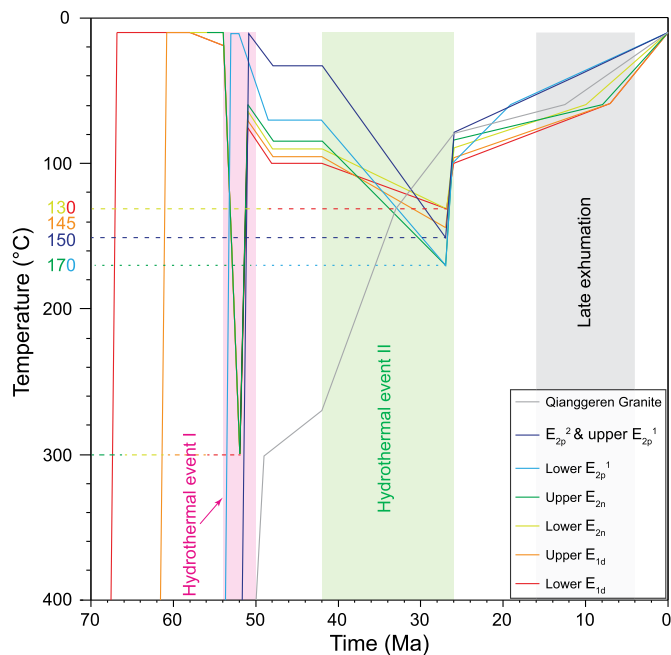
**Fig. 8.** Thermal history modeling of the Linzizong Group, associated dikes, and structurally overlying Qianggeren granite. The preferred thermal history solution of the Linzizong Groups was determined from forward modeling, whereas the best-fit thermal history of the granite was determined by inverse modeling. Numbers with different colors along the temperature axis indicate the peak temperature reached for different units of the Linzizong Group. Dashed lines with different colors are used to correlate the peak for different units of the Linzizong Group to the temperature axis.

rane. Low erosion rates are consistent with low relief landscapes (Montgomery and Brandon, 2002), which is in turn a characteristic of an internally-drained plateau; we argue that this plateau would be at moderate to high elevation considering the substantial crustal thickening of central Tibet during the Cretaceous and Paleocene time (e.g., Kapp et al., 2007). Our revised interpretation of this early Eocene ZFT and ZHe age group to represent conductive cooling after magmatic flare-up excludes the inferred large erosional exhumation and high exhumation rates for the Gangdese arc since early Eocene. Instead, together with the Cretaceous-Paleocene thermochronologic records, it supports that exhumation of the southern Lhasa terrane transformed from rapid in the Cretaceous-Paleocene to very slow in the Eocene, suggesting the development of plateau-like conditions along the southern margin of the Lhasa terrane and existence of a moderate to high Gangdese Mountain by the early Eocene.

### 5.2. Thermal event II and exhumation of the southern Lhasa terrane

We attribute thermal event II of the Linzizong Group between 42 and 27 Ma to a combination of structural burial in the footwall of the Gulu-Hamu thrust and coeval hydrothermal fluid circulation along the unconformities within the stratigraphy of the Linzhou basin. The total temperature increase of the lower $E_{1d}$, the upper $E_{1d}$, the lower $E_{2n}$, the upper $E_{2n}$, the lower $E_{2p}^1$, the upper $E_{2p}^1$ and $E_{2p}^2$ from this second thermal event, calculated by subtracting the temperature each unit reached at ∼48-42 Ma from the maximum temperature it reached at 27 Ma, is approximately 30 °C, 50 °C, 40 °C, 85 °C, 100 °C, and 115 °C (Fig. 8), respectively. The lower E1d unit was least heated during thermal event II, and its temperature increase of 30 °C can be treated uniformly as the maximum temperature increase related to structural burial for all the units. Thus, a lower limit of temperature increase solely induced by hydrothermal fluid circulation for the lower $E_{1d}$, the upper $E_{1d}$,
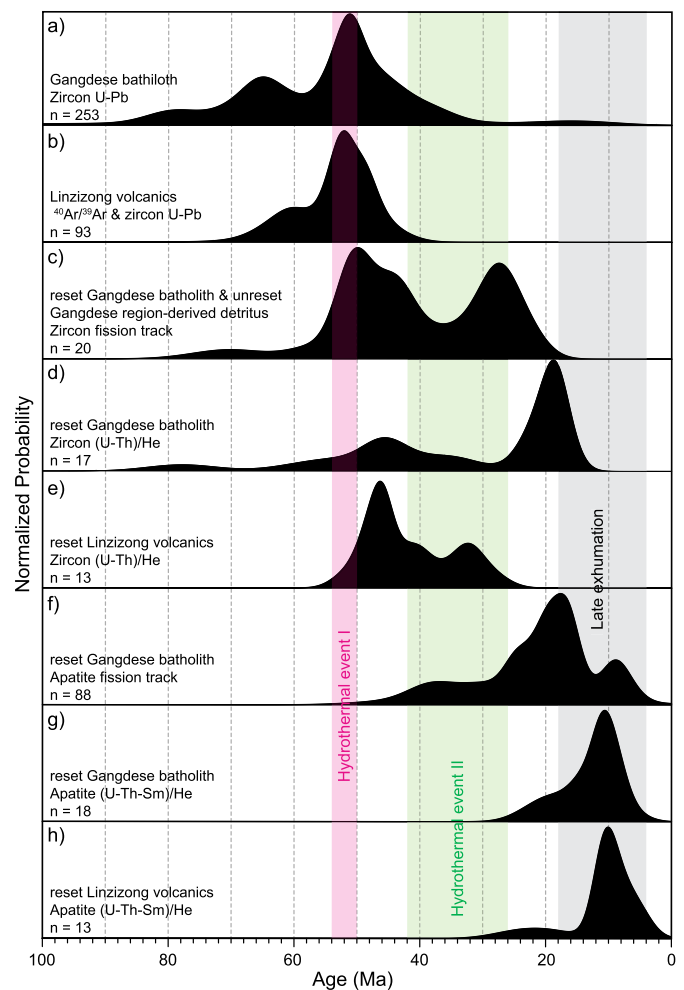


**Fig. 9.** Probability distribution functions of compiled geochronological and thermochronological data of the Gangdese batholith and Linzizong Group. Gangdese batholith zircon U-Pb ages (ages >100 Ma are not plotted) are from Zhu et al. (2015), Orme et al. (2014), and references therein; eruption ages of the Linzizong volcanic rocks are from Lee et al. (2009), Zhu et al. (2015), Chen et al. (2016), Huang et al. (2015a), Huang et al. (2015b) and references therein. Thermochronological data of the Gangdese batholith, Linzizong Group, and sediment shed from the Gangdese batholith are from Laskowski et al. (2018) and references therein, supplemented by Yuan et al. (2001), Yuan et al. (2008), Ma et al. (2017), Shen et al. (2019), and this study. Pink, green and light gray boxes are the thermal events in the Linzhou basin shown in Fig. 8.

the lower $E_{2n}$, the upper $E_{2n}$, the lower $E_{2p}^1$, the upper $E_{2p}^1$ and $E_{2p}^2$ can be estimated to be 0 °C, 20 °C, 10 °C, 55 °C, 70 °C, and 85 °C, respectively. This indicates that the hydrothermal fluid flow was the main cause of heating of the Linzizong Group, especially of the lower $E_{2p}^1$, the upper $E_{2p}^1$ and $E_{2p}^2$ units, during this second resetting event. Such a pattern of decreasing heating with depth suggests that crustal fluids emerging from the Gulu-Hamu thrust would cool as they migrated down-section, away from the thrust. Fluid flow helps explain the fast cooling of the Linzizong Group between 27 and 26 Ma when the thrust activity, and therefore faulting-induced fluid pumping (McCaig, 1988), ceased (Fig. 5a). Although we cannot estimate more precisely when this hydrothermal fluid flow initiated and how long it lasted, our restored thermal history (Fig. 8) suggests that a non-burial-related high-temperature heating event probably affected the thermochronometers during the time window of 42-27 Ma. We argue that the ZHe ages between 42 and 24 Ma of the Linzizong Group thus do not indicate rock uplift and exhumation of the Linzizong strata, but rather resetting due to migration of hydrothermal fluids through the Linzizong Group. In contrast, cooling of the Qianggeren granite was a
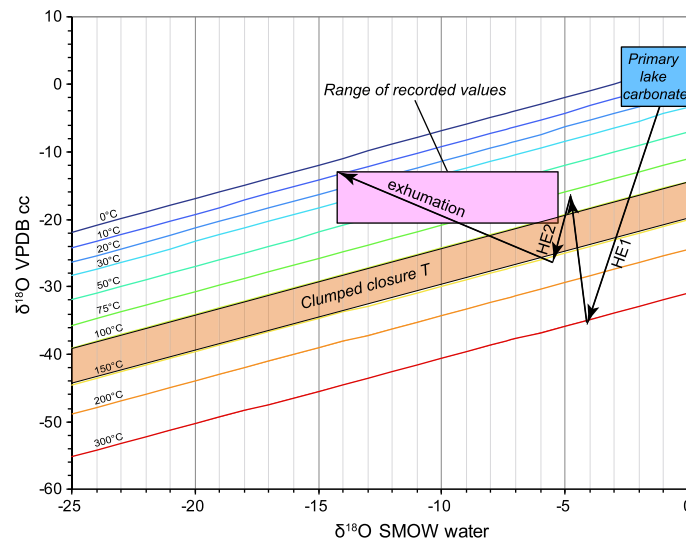
**Fig. 10.** Proposed evolution of $\delta^{18}O$ values of carbonate rock from the lower Nianbo Formation ($E_{2n}$) through Hydrothermal Events (HE) 1 and 2 discussed in text. Stable and clumped isotope results of the $E_{2n}$ are from Ingalls et al. (2018) and Quade et al. (2020). Equilibrium lines for various temperatures from 0 to 300 °C from Kim and O'Neil (1997) are also shown. The diagonal orange box encloses closure temperature of 100-150 °C for clumped isotopes. The assumed initial (primary) lake carbonate and water $\delta^{18}O$ values are enclosed in the blue box in upper righthand corner. The pink box at the center of the graph encloses the approximate range in $\delta^{18}O$ carbonate rock values and $T(\Delta_{47})$ °C measured in the $E_{2n}$ carbonates (from Ingalls et al. (2018) and Quade et al. (2020)). Arrows represent the estimated evolutionary pathway of the stable and clumped isotope results of the $E_{2n}$ based on the thermal history presented in this study. The pathway during HE1 is conjectural, since it was overprinted by HE2. VPDB, Vienna Peedee belemnite; SMOW, standard mean ocean water.

result of erosional exhumation during movement in the hanging wall of the Gulu-Hamu thrust.

The unreset ZHe ages from the upper $E_{2p}{}^{1}$ and $E_{2p}{}^{2}$ (Fig. 4) indicate that the Linzizong Group was never buried to a depth of >6 km. This conclusion is in contrast to the previous estimates that suggested the Qianggeren granite was buried by a >8 km thick Linzizong Group (He et al., 2007). The thermal history presented here better constrains the amount of the Linzizong Group removed by erosion. Our analysis suggests that the Linzizong Group was at 100-80 °C (Fig. 8) after thermal event II; this corresponds to a depth of 3.6-2.8 km if we assume a geothermal gradient of 25 °C/km. Thus, the material removed from the Linzizong Group in the Linzhou basin by erosion should be ~3 km; this is much less than the amount of overburden removed from above the Qianggeren granite samples. Our case study of the Linzhou basin emphasizes that the magnitude of Cenozoic erosional exhumation in the southern Lhasa terrane was spatially heterogeneous, and that thrust activity has been one of the main reasons for significant exhumation. This is further supported by the peak ZFT ages (~27 Ma, Fig. 9c) and ZHe ages (~19 Ma, Fig. 9d) of the Gangdese batholith located in the hanging wall of the Gangdese thrust (Ge et al., 2016; Li et al., 2016). Although thermochronologic data have been rarely reported from the Linzizong Group in other localities, thrust has not been well developed in these rocks, it is thus very likely that the Linzizong Group, or most area of the northern Gangdese arc, experienced minimal Cenozoic exhumation of ~3 km in the Neogene. In contrast, the Cenozoic exhumation is significant in the southern Gangdese arc due to the presence of a paleo-drainage divide and uplift in the hanging wall of Gangdese thrust/duplex (Laskowski et al., 2018).

*5.3. Resetting risk of primary stable and clumped isotopic records and implications for paleoaltimetry*

Our recognition of the two thermal events in the Linzhou basin has important implications for interpreting stable isotope-based paleoaltimetric data. On the one hand, consistently low $\delta^{18}O$ values averaging −14 to −18‰ (VPDB, Vienna Peedee belemnite) from the $E_{2n}$ lacustrine carbonates (pink box in Fig. 10) and upper

Pana paleosol carbonate obtained by previous studies have been interpreted as primary isotopic signals (blue box in Fig. 10) that reflect high (>4 km) paleoelevations during deposition at ca. 58-47 Ma (Ding et al., 2014; Ingalls et al., 2018). On the other hand, calcite recrystallization documented by microscopy, and $\Delta_{47}$ alteration indicated by $T(\Delta_{47})$ values ranging from 105 to 6.3 °C (pink box in Fig. 10), despite micrite preservation in some of the samples, are commonly measured in carbonates from the Linzizong Group (Ding et al., 2014; Ingalls et al., 2018; Quade et al., 2020).

The (hydro)thermal history of the Linzizong Group shown in Fig. 8 provides strong additional and independent evidence to question whether the carbonate in these strata preserved primary isotopic values (Fig. 10). This revised thermal history explains that most of the low $\delta^{18}O$ values and intermediate $T(\Delta_{47})$ (41-105 °C) estimates reflect alteration of carbonates at high water/rock ratios by hydrothermal (>50 °C) fluids (e.g., Banner and Hanson, 1990). Both theoretical and empirical evidence suggests that primary clumped isotopic compositions are not retained above clumped isotope closure temperatures of 100-150 °C of (Fig. 10) on timescales of millions of years (e.g., Passey and Henkes, 2012; Lacroix and Niemi, 2019). Magmatically-driven hydrothermal fluid circulation and heating to 300 °C during thermal event I at ~52 Ma would have reordered the clumped isotopic values in the $E_{2n}$ carbonates and likely also the $\delta^{18}O$ values (HE1 in Fig. 10). Such resetting has been documented in the southern Rocky Mountains (Abbey et al., 2018). $\delta^{18}O$ values of carbonates in the $E_{2n}$ and $E_{2p}$ may have been reset a second time during thermal event II at 42-27 Ma when they were heated to 130-170 °C (Fig. 4, HE2 in Fig. 10). Stolper and Eiler (2015) modeled the resetting of primary clumped isotopes as a two-step process in which carbonate ordering is first reset to $T(\Delta_{47})$ intermediate between surface and peak burial temperatures. These modeling results explain the intermediate $T(\Delta_{47})$ of 105-41 °C (pink box in Fig. 10) in the four lacustrine and pedogenic carbonate samples from the $E_{2n}$ in Ingalls et al. (2018), and in the 12 lacustrine carbonate samples from the $E_{2n}$ in Quade et al. (2020).

Ingalls et al. (2018) used careful petrographic selection to isolate three samples that yielded $T(\Delta_{47})$ of 6.3-11.9 °C, temperatures which were used as the basis for estimating high (>4 km) surface

elevations. The preservation of primary micritic fabrics, evidence previously used to argue against recrystallization in these three samples with low T($\Delta_{47}$) (Ingalls et al., 2018), does not preclude isotopic alteration because water-rock exchange and solid-state re-ordering can significantly alter the primary $\delta^{18}O$ and $\Delta_{47}$ without leaving textural evidence of mineral exchange (Ingalls, 2019). For example, marine carbonates of the Upper Cretaceous Takena Formation that directly underlie the Linzizong Group in this area (Fig. 1) preserve primary micritic fabrics, yet their oxygen isotopic values have been completely reset ($\delta^{18}O$ values of $-15$ to $-17‰$, much lower than a primary marine isotopic values) (Leier et al., 2009). These results are part of a much broader regional pattern of alteration to low $\delta^{18}O$ values in marine and continental carbonate rocks in the magmatically and tectonically active Gangdese arc and adjacent India-Asia suture (Quade et al., 2020). The results of our thermal history study suggest that the stable and clumped isotopic results from these three $E_{2n}$ carbonate samples should be interpreted with caution. We acknowledge that these three samples (from sections DD' and FF') are $\sim$10 km from our thermochronologic sampling localities (Fig. 1c), and thus it is likely that some carbonates were not affected by the hydrothermal alteration. Future investigations, such as subsampling distinct petrographic textures and coupled $\delta'^{18}O$-$\Delta'^{17}O$ analysis of carbonates, will verify if these carbonates with primary micrite textures in fact retain primary stable and clumped isotopic values. Our results underscore the particular challenge of obtaining primary isotopic records of paleoelevation in deep time in geologically active orogenic belts.

## 6. Conclusions

The Linzizong Group in the Linzhou basin has been widely studied to investigate the magmatism, paleolatitude, and paleoaltitude of the Gangdese arc before and during the early stages of the India-Asia collision. Here we report results of the first systematic multi-thermochronometric study of the Linzizong Group and coeval intrusive rocks (dikes and the structurally overlying Qianggeren granite). Resetting of whole rock $^{40}Ar/^{39}Ar$ ages of volcanic rocks from the $E_{1d}$ and $E_{2n}$ of the Linzizong Group indicates that they were reheated to 300 °C. ZHe ages are indistinguishable from the zircon U-Pb ages for samples from the upper $E_{2p}{}^1$ and $E_{2p}{}^2$, but they are younger than zircon U-Pb ages for samples from the $E_{1d}$, $E_{2n}$, and lower $E_{2p}{}^1$. Forward modeling of the positive ZHe ages-eU correlations, together with AHe ages reported here and previously published thermochronologic data from the Qianggeren granite, reveals that the Linzizong Group experienced two thermal events: one between 54 and 50 Ma and another between 42 and 27 Ma. The older thermal event was induced by a voluminous magmatic flare-up and associated hydrothermal fluid flow in the Linzhou region and broader Gangdese arc that peaked at $\sim$52 Ma. We argue that this pulse of magmatic heating, followed by conductive cooling, may provide a better explanation for the abundance of 45-50 Ma ZFT and ZHe ages in the Gangdese arc than rapid regional erosional exhumation induced by crustal shortening.

We attribute the $\sim$42-27 Ma thermal reheating of the Linzizong Group to 130-170 °C to a combination of structural and depositional burial during slip of the Gulu-Hamu thrust in the northern part of the Linzhou basin and coeval hydrothermal fluid flow in relatively permeable rocks and unconformities in its proximal footwall. Thermal event II and subsequent cooling suggest that exhumation of the Linzizong Group in the Linzhou basin, and perhaps elsewhere across the (northern) Gangdese arc, is limited to $\sim$3 km. In contrast, the Qianggeren granite in the hanging wall of the Gulu-Hamu thrust in the northern Linzhou basin, just a few kilometers north of the Linzizong Group described above, was exhumed from >10 km depth by rock uplift and local erosional exhumation since 42 Ma related to slip on the Gulu-Hamu thrust.

Our results and interpretation of the thermal history of the Linzizong Group are consistent with regional thermochronometric studies of the interior of the Tibetan Plateau, and together support the possibility that large part of central and southern Tibet has been characterized by very low erosion rates (and by inference low topographic relief) since 45 Ma.

Stable isotope records from carbonates in the Linzhou basin are the principal direct paleoaltimetric evidence used to argue that the Gangdese mountains were >4 km high by the early Paleogene time. Our documentation of two reheating events in the Linzhou basin since $\sim$52 Ma can explain the calcite recrystallization and $\delta^{18}O$ and $\Delta_{47}$ alteration in most carbonates from the Linzizong Group. Our study illustrates how low-temperature thermochronology may be a useful and independent tool for interrogating the preservation of primary stable isotopic records.

## CRediT authorship contribution statement

**Wentao Huang:** Conceptualization, Data curation, Formal analysis, Funding acquisition, Investigation, Methodology, Writing – original draft. **Peter C. Lippert:** Conceptualization, Writing – review & editing. **Peter W. Reiners:** Conceptualization, Formal analysis, Methodology, Writing – review & editing. **Jay Quade:** Formal analysis, Investigation, Methodology, Writing – review & editing. **Paul Kapp:** Writing – review & editing. **Morgan Ganerød:** Investigation. **Zhaojie Guo:** Resources. **Douwe J.J. van Hinsbergen:** Writing – review & editing.

## Declaration of competing interest

The authors declare that they have no known competing financial interests or personal relationships that could have appeared to influence the work reported in this paper.

## Appendix A. Supplementary material

Supplementary material related to this article can be found online at https://doi.org/10.1016/j.epsl.2022.117390.

## References

Abbey, A.L., Niemi, N.A., Geissman, J.W., Winkelstern, I.Z., Heizler, M., 2018. Early Cenozoic exhumation and paleotopography in the Arkansas River valley, southern Rocky Mountains, Colorado. Lithosphere 10, 239–266.

Ault, A.K., Frenzel, M., Reiners, P.W., Woodcock, N.H., Thomson, S.N., 2016. Record of paleofluid circulation in faults revealed by hematite (U-Th)/He and apatite fission-track dating: an example from Gower Peninsula fault fissures, Wales. Lithosphere 8, 379–385.

Banner, J.L., Hanson, G.N., 1990. Calculation of simultaneous isotopic and trace element variations during water-rock interaction with applications to carbonate diagenesis. Geochim. Cosmochim. Acta 54, 3123–3137.

Bureau of Geology and Mineral Resources of Xizang (Tibet) Autonomous Region (BGMRXAR), 1993. In: Regional Geology of Xizang (Tibet) Autonomous Region. In: Geological Memoirs Series, vol. 1. Geological Publishing House, Beijing. Number 31, 707 pp.

Cassata, W.S., Renne, P.R., 2013. Systematic variations of argon diffusion in feldspars and implications for thermochronometry. Geochim. Cosmochim. Acta 112, 251–287.

Chen, B., Ding, L., Xu, Q., Yue, Y., Xie, J., 2016. U-Pb age framework of the Linzizong volcanic rocks from the Linzhou Basin, Tibet. Quat. Sci. 36, 1037–1054.

Chen, J., Huang, B., Yi, Z., Yang, L., Chen, L., 2014. Paleomagnetic and $^{40}$Ar/$^{39}$Ar geochronological results from the Linzizong Group, Linzhou Basin, Lhasa Terrane, Tibet: implications to Paleogene paleolatitude and onset of the India-Asia collision. J. Asian Earth Sci. 96, 162–177.

Currie, B.S., Polissar, P.J., Rowley, D.B., Ingalls, M., Li, S., Olack, G., Freeman, K.H., 2016. Multiproxy paleoaltimetry of the late Oligocene-Pliocene Oiyug basin, southern Tibet. Am. J. Sci. 316, 401–436.

Ding, L., Xu, Q., Yue, Y., Wang, H., Cai, F., Li, S., 2014. The Andean-type Gangdese Mountains: paleoelevation record from the Paleocene–Eocene Linzhou Basin. Earth Planet. Sci. Lett. 392, 250–264.

Dupont-Nivet, G., Lippert, P.C., van Hinsbergen, D.J.J., Meijers, M.J.M., Kapp, P., 2010. Palaeolatitude and age of the Indo-Asia collision: palaeomagnetic constraints. Geophys. J. Int. 182, 1189–1198.

Ge, Y.-K., Dai, J.-G., Wang, C.-S., Li, Y.-L., Xu, G.-Q., Danisik, M., 2016. Cenozoic thermo-tectonic evolution of the Gangdese batholith constrained by low temperature thermochronology. Gondwana Res.

Guenthner, W.R., Reiners, P.W., Ketcham, R.A., Nasdala, L., Giester, G., 2013. Helium diffusion in natural zircon: radiation damage, anisotropy, and the interpretation of zircon (U-Th)/He thermochronology. Am. J. Sci. 313, 145–198.

He, S., Kapp, P., DeCelles, P.G., Gehrels, G.E., Heizler, M., 2007. Cretaceous-Tertiary geology of the Gangdese Arc in the Linzhou area, southern Tibet. Tectonophysics 433, 15–37.

Hu, X., Garzanti, E., Moore, T., Raffi, I., 2015. Direct stratigraphic dating of India-Asia collision onset at the Selandian (middle Paleocene, 59±1 Ma). Geology 43, 859–862.

Huang, W., Dupont-Nivet, G., Lippert, P.C., van Hinsbergen, D.J.J., Dekkers, M.J., Waldrip, R., Ganerød, M., Li, X., Guo, Z., Kapp, P., 2015a. What was the Paleogene latitude of the Lhasa terrane? A reassessment of the geochronology and paleomagnetism of Linzizong volcanic rocks (Linzhou Basin, Tibet). Tectonics 34, 594–622. https://doi.org/10.1002/2014TC003787.

Huang, W., Dupont-Nivet, G., Lippert, P.C., van Hinsbergen, D.J.J., Dekkers, M.J., Guo, Z., Waldrip, R., Li, X., Zhang, X., Liu, D., Kapp, P., 2015b. Can a primary remanence be retrieved from partially remagnetized Eocence volcanic rocks in the Nanmulin Basin (southern Tibet) to date the India-Asia collision? J. Geophys. Res., Solid Earth 120, 42–66. https://doi.org/10.1002/2014JB011599.

Ingalls, M., 2019. Reconstructing carbonate alteration histories in orogenic sedimentary basins: Xigaze forearc, southern Tibet. Geochim. Cosmochim. Acta 251, 284–300.

Ingalls, M., Rowley, D., Olack, G., Currie, B., Li, S., Schmidt, J., Tremblay, M., Polissar, P., Shuster, D.L., Lin, D., 2018. Paleocene to Pliocene low-latitude, high-elevation basins of southern Tibet: implications for tectonic models of India-Asia collision, Cenozoic climate, and geochemical weathering. Geol. Soc. Am. Bull. 130, 307–330.

Kapp, P., DeCelles, P.G., Gehrels, G.E., Heizler, M., Ding, L., 2007. Geological records of the Lhasa-Qiangtang and Indo-Asian collisions in the Nima area of central Tibet. Geol. Soc. Am. Bull. 119, 917–933.

Ketcham, R.A., 2005. Forward and inverse modeling of low-temperature thermochronometry data. Rev. Mineral. Geochem. 58, 275–314.

Khan, M.A., Spicer, R.A., Bera, S., Ghosh, R., Yang, J., Spicer, T.E., Guo, S.-x., Su, T., Jacques, F., Grote, P.J., 2014. Miocene to Pleistocene floras and climate of the Eastern Himalayan Siwaliks, and new palaeoelevation estimates for the Namling–Oiyug Basin, Tibet. Glob. Planet. Change 113, 1–10.

Kim, S.-T., O'Neil, J.R., 1997. Equilibrium and nonequilibrium oxygen isotope effects in synthetic carbonates. Geochim. Cosmochim. Acta 61, 3461–3475.

Lacroix, B., Niemi, N.A., 2019. Investigating the effect of burial histories on the clumped isotope thermometer: an example from the Green River and Washakie Basins, Wyoming. Geochim. Cosmochim. Acta 247, 40–58.

Laskowski, A.K., Kapp, P., Cai, F., 2018. Gangdese culmination model: Oligocene–Miocene duplexing along the India-Asia suture zone, Lazi region, southern Tibet. Geol. Soc. Am. Bull.

Lee, H.Y., Chung, S.-L., Wang, Y., Zhu, D., Yang, J., Song, B., Liu, D., Wu, F., 2007. Age, petrogenesis and geological significance of the linzizong volcanic successions in the Linzhou basin, southern Tibet: evidence from zircon U-Pb dates and Hf isotopes. Acta Petrol. Sin. 23, 493–500.

Lee, H.Y., Chung, S.L., Lo, C.H., Ji, J., Lee, T.Y., Qian, Q., Zhang, Q., 2009. Eocene Neotethyan slab breakoff in southern Tibet inferred from the Linzizong volcanic record. Tectonophysics 477, 20–35.

Leier, A., Quade, J., DeCelles, P., Kapp, P., 2009. Stable isotopic results from paleosol carbonate in South Asia: paleoenvironmental reconstructions and selective alteration. Earth Planet. Sci. Lett. 279, 242–254.

Li, G., Kohn, B., Sandiford, M., Xu, Z., Tian, Y., Seiler, C., 2016. Synorogenic morphotectonic evolution of the Gangdese batholith, South Tibet: insights from low-temperature thermochronology. Geochem. Geophys. Geosyst. 17, 101–112. https://doi.org/10.1002/2015GC006047.

Licht, A., van Cappelle, M., Abels, H.A., Ladant, J.B., Trabucho-Alexandre, J., France-Lanord, C., Donnadieu, Y., Vandenberghe, J., Rigaudier, T., Lecuyer, C., Terry Jr, D., Adriaens, R., Boura, A., Guo, Z., Soe, A.N., Quade, J., Dupont-Nivet, G., Jaeger, J.J., 2014. Asian monsoons in a late Eocene greenhouse world. Nature 513, 501–506.

Ma, Y., Xu, Z., Li, G., Ma, S., Ma, X., Chen, X., Zhao, Z., 2017. Crustal deformation of the Gangdese Cretaceous back-arc basin and formation of Proto-plateau, South Tibet. Acta Petrol. Sin. 33, 3861–3872.

McCaig, A.M., 1988. Deep fluid circulation in fault zones. Geology 16, 867–870.

Molnar, P., England, P., Martinod, J., 1993. Mantle dynamics, uplift of the Tibetan Plateau, and the Indian monsoon. Rev. Geophys. 31, 357–396.

Montgomery, D.R., Brandon, M.T., 2002. Topographic controls on erosion rates in tectonically active mountain ranges. Earth Planet. Sci. Lett. 201, 481–489.

Orme, D.A., Carrapa, B., Kapp, P., 2014. Sedimentology, provenance and geochronology of the upper Cretaceous–lower Eocene western Xigaze forearc basin, southern Tibet. Basin Res. 1 (25). https://doi.org/10.1111/bre.12080.

Passey, B.H., Henkes, G.A., 2012. Carbonate clumped isotope bond reordering and geospeedometry. Earth Planet. Sci. Lett. 351, 223–236.

Quade, J., Leary, R., Dettinger, M.P., Orme, D.A., Krupa, A., DeCelles, P.G., Kano, A., Kato, H., Waldrip, R., Huang, W., Kapp, P., 2020. Resetting southern Tibet: the serious challenge of obtaining primary records of paleoaltimetry. Glob. Planet. Change 191, 103194.

Raymo, M.E., Ruddiman, W.F., 1992. Tectonic forcing of late Cenozoic climate. Nature, 117–122.

Reiners, P.W., Spell, T.L., Nicolescu, S., Zanetti, K.A., 2004. Zircon (U-Th)/He thermochronometry: He diffusion and comparisons with 40Ar/39Ar dating. Geochim. Cosmochim. Acta 68, 1857–1887.

Rohrmann, A., Kapp, P., Carrapa, B., Reiners, P.W., Guynn, J., Ding, L., Heizler, M., 2012. Thermochronologic evidence for plateau formation in central Tibet by 45 Ma. Geology 40, 187–190.

Rowley, D.B., Currie, B.S., 2006. Palaeo-altimetry of the late Eocene to Miocene Lunpola basin, central Tibet. Nature 439, 677–681. https://doi.org/10.1038/nature04506.

Shen, T., Wang, G., Bernet, M., Replumaz, A., Ai, K., Song, B., Zhang, K., Zhang, P., 2019. Long-term exhumation history of the Gangdese magmatic arc: implications for the evolution of the Kailas Basin, western Tibet. Geol. J.

Stolper, D.A., Eiler, J.M., 2015. The kinetics of solid-state isotope-exchange reactions for clumped isotopes: a study of inorganic calcites and apatites from natural and experimental samples. Am. J. Sci. 315, 363–411.

Su, T., Farnsworth, A., Spicer, R., Huang, J., Wu, F.-X., Liu, J., Li, S.-F., Xing, Y.-W., Huang, Y.-J., Deng, W.-Y.-D., 2019. No high Tibetan Plateau until the Neogene. Sci. Adv. 5. eaav2189.

Wang, E., Kamp, P.J., Xu, G., Hodges, K.V., Meng, K., Chen, L., Wang, G., Luo, H., 2015. Flexural bending of southern Tibet in a retro foreland setting. Sci. Rep. 5, 12076.

Wei, Y., Zhang, K., Garzione, C.N., Xu, Y., Song, B., Ji, J., 2016. Low palaeoelevation of the northern Lhasa terrane during late Eocene: fossil foraminifera and stable isotope evidence from the Gerze Basin. Sci. Rep. 6, 27508.

Yuan, W., Deng, J., Zheng, Q., Dong, J., Bao, Z., Eizenhoefer, P.R., Xu, X., Huang, Z., 2008. Apatite fission track constraints on the Neogene tectono-thermal history of Nimu area, southern Gangdese terrane, Tibet Plateau. Isl. Arc 18, 488–495.

Yuan, W., Wang, S., Li, S., Yang, Z., 2001. Apatite fission track dating evidence on the tectonization of Gangdese block, south Qinghai-Tibetan Plateau. Chin. Sci. Bull. 47, 240–244.

Yue, Y., Ding, L., 2006. $^{40}$Ar/$^{39}$Ar geochronology, geochemical characteristics and genesis of the Linzhou basic dikes, Tibet. Acta Petrol. Sin. 22, 855–866.

Zhou, S., Mo, X., Dong, G., Zhao, Z., Qiu, R., Guo, T., Wang, L., 2004. $^{40}$Ar/$^{39}$Ar geochronology of Cenozoic Linzizong volcanic rocks from Linzhou Basin, Tibet, China, and their geological implications. Chin. Sci. Bull. 49, 1970–1979.

Zhu, D.-C., Wang, Q., Zhao, Z.-D., Chung, S.-L., Cawood, P.A., Niu, Y., Liu, S.-A., Wu, F.-Y., Mo, X.-X., 2015. Magmatic record of India-Asia collision. Sci. Rep. 5, 14289. https://doi.org/10.1038/srep14289.